British Journal of Pharmacology (2005) 146, 146–161 © 2005 Nature Publishing Group All rights reserved 0007–1188/05 $30.00
www.nature.com/bjp

Spironolactone and its main metabolite canrenoic acid block hKv1.5, Kv4.3 and Kv7.1 + minK channels

[1]Ricardo Gómez, [1]Lucía Núñez, *,[1]Ricardo Caballero, [1]Miguel Vaquero, [1]Juan Tamargo & [1]Eva Delpón

[1]Department of Pharmacology, School of Medicine, Universidad Complutense, 28040 Madrid, Spain

1 Both spironolactone (SP) and its main metabolite, canrenoic acid (CA), prolong cardiac action potential duration and decrease the Kv11.1 (HERG) current. We examined the effects of SP and CA on cardiac hKv1.5, Kv4.3 and Kv7.1 + minK channels that generate the human I_{Kur}, I_{to1} and I_{Ks}, which contribute to the control of human cardiac action potential duration.

2 hKv1.5 currents were recorded in stably transfected mouse fibroblasts and Kv4.3 and Kv7.1 + minK in transiently transfected Chinese hamster ovary cells using the whole-cell patch clamp.

3 SP (1 μM) and CA (1 nM) inhibited hKv1.5 currents by 23.2 ± 3.2 and 18.9 ± 2.7%, respectively, shifted the midpoint of the activation curve to more negative potentials and delayed the time course of tail deactivation.

4 SP (1 μM) and CA (1 nM) inhibited the total charge crossing the membrane through Kv4.3 channels at + 50 mV by 27.1 ± 6.4 and 27.4 ± 5.7%, respectively, and accelerated the time course of current decay. CA, but not SP, shifted the inactivation curve to more hyperpolarised potentials (V_h −37.0 ± 1.8 vs −40.8 ± 1.6 mV, $n = 10$, $P < 0.05$).

5 SP (10 μM) and CA (1 nM) also inhibited Kv7.1 + minK currents by 38.6 ± 2.3 and 22.1 ± 1.4%, respectively, without modifying the voltage dependence of channel activation. SP, but not CA, slowed the time course of tail current decay.

6 CA (1 nM) inhibited the I_{Kur} (29.2 ± 5.5%) and the I_{to1} (16.1 ± 3.9%) recorded in mouse ventricular myocytes and the I_K (21.8 ± 6.9%) recorded in guinea-pig ventricular myocytes.

7 A mathematical model of human atrial action potentials demonstrated that K^+ blocking effects of CA resulted in a lengthening of action potential duration, both in normal and atrial fibrillation simulated conditions.

8 The results demonstrated that both SP and CA directly block hKv1.5, Kv4.3 and Kv7.1 + minK channels, CA being more potent for these effects. Since peak free plasma concentrations of CA ranged between 3 and 16 nM, these results indicated that blockade of these human cardiac K^+ channels can be observed after administration of therapeutic doses of SP.

9 Blockade of these cardiac K^+ currents, together with the antagonism of the aldosterone proarrhythmic effects produced by SP, might be highly desirable for the treatment of supraventricular arrhythmias.

British Journal of Pharmacology (2005) **146,** 146–161. doi:10.1038/sj.bjp.0706302;
published online 27 June 2005

Keywords: Spironolactone; canrenoic acid; cardiac potassium channels; hKv1.5; Kv4.3; Kv7.1 + minK; patch clamp; repolarisation

Abbreviations: AF, atrial fibrillation; CA, canrenoic acid; CHO, Chinese hamster ovary cells; HERG, human ether-a-go-go-related gene; I_{Kr}, rapid component of the delayed rectifier current; I_{Ks}, slow component of the delayed rectifier current; I_{Kur}, ultrarapid delayed rectifier current; I_{to1}, 4-aminopyridine-sensitive component of the transient outward current; KChIP2, K^+ channel interacting protein; Ltk^- cells, mouse fibroblasts; MiRP1, minK-related peptide; RALES, Randomised Aldactone Evaluation Study; SP, spironolactone

Introduction

Aldosterone receptor antagonists, like spironolactone (SP) and eplerenone, have become increasingly more important since it has been demonstrated that aldosterone produces cardiac and vascular fibrosis, left ventricular hypertrophy, congestive heart failure, hypertension, endothelial dysfunction and cardiac arrhythmias (Stier *et al*., 2002). Furthermore, aldosterone also potentiates the effects of catecholamines, blunts baroreflex response and produces sodium retention, and potassium and magnesium depletion (Stier *et al*., 2002). The Randomised Aldactone Evaluation Study (RALES) has shown that the addition of a low dose of SP on top of an angiotensin-converting enzyme inhibitor, a loop diuretic and, in most cases, digoxin, results in a 30% reduction in mortality in patients with severe congestive heart failure (Pitt *et al*., 1999). This reduction was attributed to a lower risk of both death from progressive heart failure and sudden death from cardiac causes. Furthermore, SP reduced the heart rate, improved

*Author for correspondence; E-mail: rcaballero@ift.csic.es

heart rate variability and QT dispersion in chronic heart failure (Yee *et al*., 2001), and decreased the incidence of ventricular arrhythmia in patients with congestive heart failure secondary to idiopathic-dilated or ischaemic cardiomyopathy (Ramires *et al*., 2000). These effects of SP have been attributed to the antagonism of aldosterone proarrhythmic effects at the receptor level.

In the human myocardium, the duration of the action potential is largely determined by several outward K^+ currents, including (Tamargo *et al*., 2004): (a) the 4-aminopyridine-sensitive component of the transient outward current (I_{to1}) carried by Kv4.3 α-subunits co-assembled with K^+ channel interacting proteins (KChIP2) β-subunits; (b) the rapidly activating slowly inactivating delayed rectifier current (I_{Kur}) generated by hKv1.5 channels and (c) the slow (I_{Ks}) and the fast (I_{Kr}) components of the delayed rectifier current. Coassembly of Kv7.1 (KvLQT1) with minK produces the I_{Ks} current, whereas the I_{Kr} current is carried by channels formed by the coassembly of human ether-a-go-go-related gene (HERG) Kv11.1 α-subunits and minK-related peptide (MiRP1) β-subunits. The configuration and the action potential duration vary considerably among different cardiac regions (atria vs ventricle) and specific areas within those regions (epicardium vs endocardium) (Antzelevitch & Fish, 2001; Nerbonne & Guo, 2002). This heterogeneity mainly reflects differences in the type and/or expression patterns of the K^+ channels. It is currently assumed that I_{Kr} plays a critical role in the control of human ventricular repolarisation and QT duration, whereas I_{Kur} is only recorded in human atria.

SP is extensively metabolised in man, leading to the formation of many different metabolites, which have been divided into two main categories: those in which the sulphur of SP is retained and those in which the sulphur is removed (Figure 1) (Karim, 1978). The former molecules are considered minor metabolites and are barely detected in humans. However, about 79% of the SP oral dose is converted by dethioacetylation to canrenone, its major biologically active metabolite. Canrenone undergoes hydrolysis of its γ-lactone ring to canrenoic acid (CA). Thus, after equilibrium, similar plasma concentrations of CA and canrenone are reached. Recently, it has been demonstrated that SP and CA, at therapeutic concentrations, decreased the Kv11.1 current (Caballero *et al*., 2003). However, the effects of SP and CA on hKv1.5, Kv4.3 and Kv7.1 + minK channels are unknown. Thus, the present study was undertaken to analyse whether SP and CA modify channels hKv1.5, Kv4.3 and Kv7.1 + minK expressed in mammalian cell lines.

Methods

Cell culture

Cell culture of mouse fibroblast or *Ltk*$^-$ cells stably expressing hKv1.5 channels has been described in detail elsewhere (Caballero *et al*., 2001; 2003; Moreno *et al*., 2003). Transfected cells were cultured in Dulbecco's modified Eagle medium (Sigma Chemical Co., London, U.K.) supplemented with 10% horse serum and 0.25 mg ml^{-1} G418 (a neomycin analog; Gibco, Grand Island, NY, U.S.A.) in a 5% CO_2 atmosphere. Prior to experimental use, subconfluent cultures were incubated with 2 μM dexamethasone for 24 h as expression of the channel was under control of a dexamethasone-inducible promoter (Snyders *et al*., 1993). Chinese hamster ovary cells (CHO) were grown in Hams-F12 medium with 10% foetal bovine serum and transiently transfected with the cDNA encoding the Kv7.1 and minK (1.6 and 0.8 μg, respectively) or the Kv4.3 (3 μg) channels together with the cDNA encoding

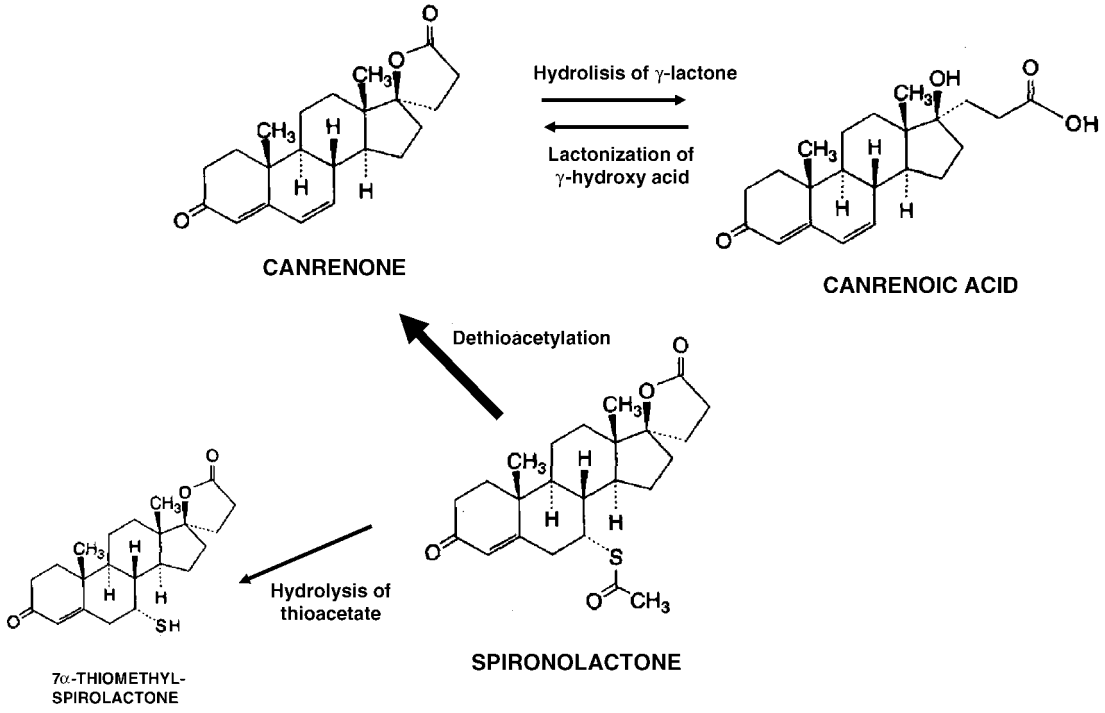

Figure 1 Schematic diagram showing the initial steps of the two main pathways of biotransformation of SP in the human liver.

the CD8 antigen (0.5 μg) by use of lipofectamine (Gibco). Before experimental use, cells were incubated with polystyrene microbeads precoated with an anti-CD8 antibody (Dynabeads M450; Dynal, Norway). Most of the cells that were beaded also had channel expression (Caballero *et al*., 2001; Moreno *et al*., 2003). Only beaded cells were used for electrophysiological recording.

Isolation of myocytes

Single ventricular myocytes were obtained from hearts of adult male CD-1 mice ($\approx$30 g) and guinea-pigs (250–300 g) by enzymatic dissociation following procedures previously described (Caballero *et al*., 2003; Brouillette *et al*., 2004; Brunet *et al*., 2004). Animals were heparinised, anaesthetised and killed following the Guidelines for Animal Care and Use of Laboratory Animals described in the Directive 86/609/EEC published in 1986 by the Council of the European Communities.

Solutions and drugs

A small aliquot of cell suspension was placed in a chamber mounted on the stage of an inverted microscope (Nikon TMS; Nikon Co., Tokyo, Japan). After settling to the bottom of the chamber, *Ltk*$^-$ and CHO cells were superfused with an 'external' solution containing (mM): NaCl 130, KCl 4, $CaCl_2$ 1, $MgCl_2$ 1, HEPES 10 and glucose 10 (pH = 7.4 with NaOH). Mouse and guinea-pig ventricular myocytes were superfused with an external solution containing (mM): NaCl 140, KCl 4, $CaCl_2$ 1, $MgCl_2$ 1, glucose 10, HEPES-Na 10, tetrodotoxin 0.03 and $CoCl_2$ 2 (pH = 7.4 with NaOH). Recording pipettes were filled with an 'internal' solution containing (mM): K-aspartate 80, KCl 42, KH_2PO_4 10, MgATP 5, phosphocreatine 3, HEPES 5 and EGTA 5 (pH = 7.2 with KOH). When analysing Kv7.1 + minK currents, phosphatidylinositol 4,5-diphosphate (5 μg ml^{-1}) was added to the internal solution to avoid the rundown of the current (Loussouarn *et al*., 2003). SP and CA (Sigma) were dissolved in dimethyl sulphoxide and methanol, respectively, to make 10 mM stock solution. Further dilutions were carried out in external solution to obtain the desired final concentration immediately before each experiment. Control solutions contained the same dimethyl sulphoxide or methanol concentrations as the test solution.

Recording techniques

hKv1.5, Kv4.3, Kv7.1 + minK and outward K^+ currents from mouse ventricular myocytes were recorded using the whole-cell configuration of the patch-clamp technique. I_K currents from guinea-pig ventricular myocytes were recorded using the perforated-nystatin patch configuration of the patch-clamp technique (Delpón *et al*., 1995; Caballero *et al*., 2003).

Under our experimental conditions, hKv1.5 and Kv4.3 current amplitudes remained unchanged during the time of recordings (25–30 min) (Caballero *et al*., 2004). Stability of Kv7.1 + minK currents is here demonstrated (see Results). Currents were recorded at room temperature using Axopatch 200B patch-clamp amplifiers (Axon Instruments; Foster City, CA, U.S.A.). Pipettes were pulled from Narishige borosilicate capillary tubes (GD1; Narishige Co. Ltd, Tokyo, Japan) using a programmable patch micropipette puller (P-87, Sutter Instruments Co., Novato, CA, U.S.A.) and were heat polished with a microforge (MF-83, Narishige). To ensure voltage-clamp quality, micropipette resistance was kept below 3.5 MΩ when filled with the internal solution and immersed in the external solution. The capacitive transients elicited by symmetrical 10 mV steps were recorded at 50 kHz (filtered at 10 kHz) for subsequent calculation of capacitive surface area, access resistance and input impedance. Maximum hKv1.5 current amplitudes in *Ltk*$^-$ cells averaged 1.4 $\pm$ 0.3 nA, access resistance 4.3 $\pm$ 0.2 MΩ, and cell capacitance 9.9 $\pm$ 1.2 pF (n = 12). In CHO cells capacitance averaged 14.9 $\pm$ 0.7 pF and access resistance 4.5 $\pm$ 0.2 MΩ (n = 22). Maximum Kv7.1 + minK and Kv4.3 currents averaged 1.1 $\pm$ 0.2 and 2.5 $\pm$ 0.4 nA (n = 11), respectively. Typically $\approx$80% of capacitance and series resistance could be compensated, which leads to mean uncompensated access resistances of 2.6 $\pm$ 0.4 and 1.7 $\pm$ 0.1 MΩ for *Ltk*$^-$ and CHO cells, respectively. Mean capacitance, access resistance and uncompensated access resistance of mouse ventricular myocytes were 238 $\pm$ 13 pF, 4.0 $\pm$ 0.6 and 1.7 $\pm$ 0.4 MΩ (n = 8), respectively. In guinea-pig ventricular myocytes, the effective access resistance and the maximum current amplitude were 13.7 $\pm$ 1.1 MΩ and 239.9 $\pm$ 24.1 pA, respectively (n = 5). Thus, under these conditions no significant voltage errors (< 5 mV) due to series resistance were expected with the electrodes used. Moreover, the low capacitance enabled fast-clamp control. The current records were sampled at 3–10 times the antialias filter setting and stored on the hard disk of a computer for subsequent analysis. Data acquisition and command potentials were controlled by pCLAMP 9.0 software (Axon Instruments).

Pulse protocols and analysis

After control data had been obtained, bath perfusion was switched to a drug-containing solution. Thereafter, an equilibration period of 7–10 min was allowed to elapse before measuring the drug effects. The holding potential was maintained at $-$80 mV and the cycle time for any protocol was 10 s to avoid accumulation of inactivation and/or block. The protocol to obtain current–voltage relationships consisted of 250-ms (Kv4.3), 500-ms (hKv1.5) or 2000-ms (Kv7.1 + minK) pulses that were imposed in 10 mV increments between $-$80 and + 60 mV (hKv1.5) or + 40 mV (Kv7.1 + minK) and from $-$90 to + 50 mV (Kv4.3). Between $-$80 and $-$40 mV, only passive linear leak was observed and least-squares fits to these data were used for passive leak correction. Deactivating hKv1.5 and Kv7.1 + minK 'tail' currents were recorded on return to $-$40 mV.

The activation curves of hKv1.5 and Kv7.1 + minK currents were constructed by plotting tail current amplitudes elicited as a function of the membrane potential and fitted with a Boltzmann distribution according to the following equation:

$$y = A/\{1 + \exp[(V_h - V_m)/k]\} \quad (1)$$

where A is the amplitude term, V_h is the midpoint of activation, V_m is the test potential and k represents the slope factor for the activation curve.

To describe the time course of current activation upon depolarisation, as well as the tail currents upon repolarisation, exponential analysis was used as an operational approach,

fitting the current traces to an equation of the form:

$$y = C + A_1 \exp(-t/\tau_1) + A_2 \exp(-t/\tau_2) + \cdots + A_n \exp(-t/\tau_n) \quad (2)$$

where τ_1, τ_2 and τ_n are the system time constants, A_1, A_2 and A_n are the amplitudes of each component of the exponential, and C is the baseline value. The curve-fitting procedure used a nonlinear least-squares (Gauss–Newton) algorithm; results were displayed in linear and semilogarithmic format, together with the difference plot. Goodness of fit was judged by the χ^2 criterion and by inspection for systematic nonrandom trends in the difference plot.

To obtain the IC_{50} (concentration of drug that produces the half maximum inhibition) and the Hill coefficient, n_H, the fractional block obtained at various drug concentrations [D] was fitted to the equation:

$$f = 1/\{1 + (IC_{50} + /[D])^{n_H}\} \quad (3)$$

In mouse ventricular myocytes, in a first group of experiments, outward K^+ currents were recorded in cells previously superfused with 4-aminopyridine (50 μM) by applying 250-ms pulses from -80 mV to potentials ranging from -90 to $+50$ mV. Under these conditions, I_{Kur} would be inhibited (Tamargo *et al*., 2004), leaving a transient current that rapidly activated and decayed to a constant level at the end of the pulse that is mainly composed of I_{to1}, carried through Kv4.3 channels (Brunet *et al*., 2004). In another group of experiments, after a 200-ms prepulse to $+40$ mV to inactivate the transient component, 500-ms pulses to $+50$ mV were applied. Using this protocol, a slowly inactivating delayed rectifier outward K^+ current, which is composed of I_{Kur} (encoded by hKv1.5 channels) and I_{ss} encoded by Kv2.1 channels (Brunet *et al*., 2004), was obtained. Since Kv2.1 currents do not inactivate, we considered the inactivating component of this current as a result of the decay of the current carried by Kv1.5 channels and thus, the current amplitude was measured as the difference between the peak current and the current at the end of the pulse. Using this procedure, Kv1.5 current amplitude is somewhat underestimated, and the blockade values should be considered as approximate, since it is not easy to accurately determine the participation of each component in the total current amplitude (Brunet *et al*., 2004). In guinea-pig ventricular myocytes, I_K was recorded by applying 5-s pulses to $+30$ mV and tail currents were elicited upon repolarisation to -30 mV.

Mathematical modelling of a human atrial action potential

For simulating the shapes of human atrial action potentials (APs), we employed a mathematical model previously described (Courtemanche *et al*., 1999). This model also described the electrophysiological remodelling in chronic atrial fibrillation (AF) (70% reduction in $I_{Ca,L}$, and 50% reduction in I_{to1} and I_{Kur}). Changes of membrane potential were calculated for space-clamp conditions as follows:

$$dV_m/dt = -(I_{ion} + I_{st})/C_m \quad (4)$$

where $I_{ion} = I_{Na} + I_{Ca,L} + I_{to1} + I_{Kur} + I_{Kr} + I_{Ks} + I_{K1} + I_{b,Ca} + I_{b,Na} + I_{NaCa} + I_{p,Ca} + I_{Na,K}$, I_{st} is the stimulus current of 10 μA μF^{-1} applied 0.5 ms at the beginning of each cycle, and C_m is the membrane capacitance (specific C_m assumed to be 1 μF cm^{-2}). Numerical integration of $d(V_m)/dt$ was performed using the ode15s algorithm that integrates the system of differential equations given a time interval and a set of initial conditions. Simulated APs, currents and ionic concentrations were allowed to stabilise for at least 200 cycles and were implemented in MATLAB 6.5 (The MathWorks, Natick, Mass, U.S.A.).

The model was run for normal conditions and for AF-modified conditions, simulating the electrical remodelling, at pacing frequencies of 1 Hz (Courtemanche *et al*., 1999). It was then run considering the observed effects of CA 1 nM on Kv4.3 (I_{to1}), hKv1.5 (I_{Kur}), Kv11.1 (I_{Kr}) and Kv7.1 + minK (I_{Ks}) by reducing the specific conductance of each channel. Besides, the activation and inactivation time courses were also modified to reflect the experimentally registered changes.

Statistical methods

Data obtained after drug exposure were compared with those obtained under control conditions in a paired manner. For comparisons at a single voltage, differences were analysed using the Student's t-test. To analyse block at multiple voltages, two-way analysis of variance was used followed by Newman–Keuls test. Results are expressed as mean ± s.e.m. A P-value of less than 0.05 was considered as significant. More details on each procedure are given under 'Results'.

Results

Effects of SP and CA on hKv1.5 currents

In Figure 2, families of current traces are shown for control conditions and after perfusion of 1 μM SP (panel a) and 1 nM CA (panel b) obtained by applying 500-ms pulses from -80 mV to voltages between -80 and $+60$ mV in 10 mV increments. Tail currents were recorded on repolarisation to -40 mV for 500 ms (insets). At these concentrations, SP and CA did not significantly modify the peak current amplitude and the time constant of current activation (0.9 ± 0.1 ms, $n = 20$). However, both drugs slightly decreased the current amplitude measured at the end of the depolarising pulses without modifying the time course of current inactivation. In fact, the time constant of current inactivation, calculated by fitting the current traces elicited at $+60$ mV by a monoexponential function, averaged 209 ± 17 ms, whereas in the presence of SP and CA they averaged 195 ± 17 and 221 ± 15 ms, respectively ($n = 12$, $P > 0.05$). The time course of tail currents elicited upon repolarisation after pulses to $+60$ mV was fitted by a biexponential function (Table 1). SP and CA decreased the peak tail current amplitude (insets in Figure 2) and slowed the time course of deactivation (Table 1). The effects of SP (not shown) and CA were reversible in a 98.8 ± 1.2 and 99.3 ± 0.8%, respectively, upon 7–10 min washout (upper part of Figure 2b) with drug-free solution. To analyse the time course of development of SP- and CA-induced block on hKv1.5 currents, a well-established method previously reported by many investigators was followed (Castle, 1990; Carmeliet, 1992; Duan *et al*., 1993; Delpón *et al*., 1995). First we obtained the drug-sensitive current ($I_{CON} - I_{DRUG}$) by the digital subtraction of the control current

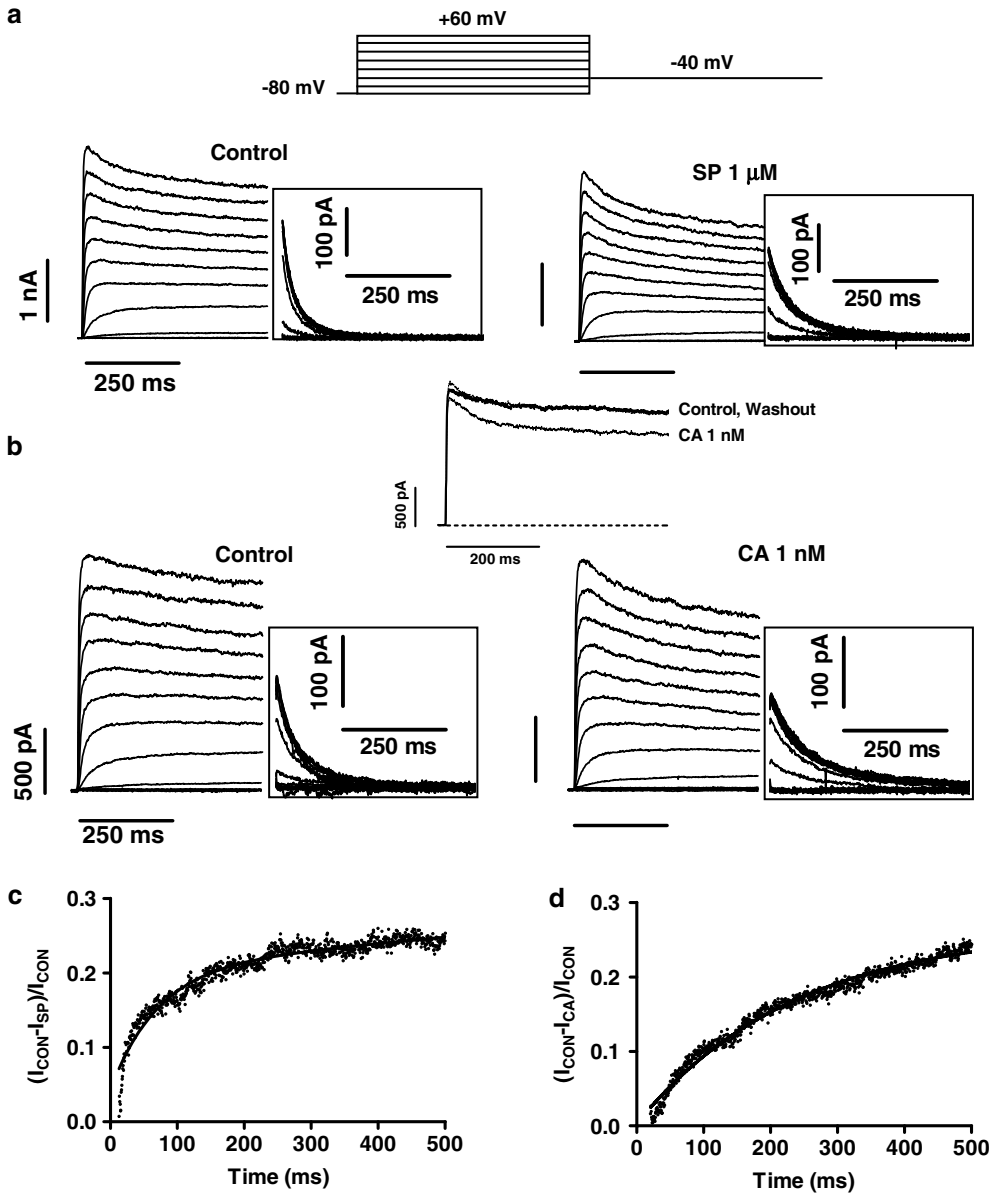

Figure 2 (a, b) hKv1.5 current traces obtained with the voltage protocol illustrated in the upper part for control conditions and with 1 μM SP (a) or 1 nM CA (b). (c, d) Plot of the current ratio between the SP- and CA-sensitive currents during the pulse to +60 mV ($I_{CON}-I_{SP}$ and $I_{CON}-I_{CA}$, respectively) and the current in control conditions. The continuous line in both panels represents the fit to a monoexponential function to obtain the τ_{block}. SP, spironolactone; CA, canrenoic acid.

trace elicited at +60 mV and the current trace recorded in the presence of the drug. Thereafter, the drug-sensitive current was digitally divided by the current trace in control conditions [$(I_{CON}-I_{DRUG})/I_{CON}$]. Following this procedure, the kinetics of the development of block appeared without any interference of the time dependence of the activation/inactivation of the channel. The ratios between the SP- and CA-sensitive currents and the current in control conditions are shown in Figures 2c and d, respectively, where an initial value of 0.0 indicates no block. In both cases, the blockade monotonically increased during the application of the depolarising pulse. Thus, the onset of block was fitted by a single exponential function (solid line) to determine the time constant of development of block (τ_{block}), which averaged 133.7±62.2 and 249.3±34.2 ms in the presence of 1 μM SP and 1 nM CA, respectively.

SP and CA inhibited hKv1.5 currents in a concentration-dependent (Figures 3a and d) manner. The reduction of the current after 500 ms at +60 mV was fitted to the Hill equation, and yielded IC_{50} and n_H values of 134.7±31.2 μM and 0.3±0.09 and 173.5±21.6 μM and 1.5±0.4 for SP and CA, respectively. As can be observed, in the presence of CA the blockade remained almost unchanged in the range of concentrations between 0.01 nM and 1 μM, and, thereafter, it increased as the CA concentration was increased. In an attempt to better define the CA concentration–response curve, blockade elicited after pulses to 0 mV and at the peak tail currents elicited on return to −40 mV after pulses to +60 mV were also plotted as a function of the CA concentration (Figure 3d). The shape of the concentration–response curves obtained with these procedures was similar to that obtained

Table 1 Effects of SP and CA on the characteristics of hKv1.5, Kv4.3 and Kv7.1 + minK currents

Current						
hKv1.5	*Control*	*SP (1 μM)*	*Control*	*CA (1 nM)*	*Control*	*CA (500 μM)*
$\tau_{f\,deactivation}$ (ms)	25.9±4.9	38.5±7.3*	30.2±2.6	48.9±5.1**	34.3±7.1	77.2±26.1**
$\tau_{s\,deactivation}$ (ms)	105.1±24.3	160.8±39.9*	103.5±15.4	154.8±24.6	95.9±5.0	275.1±42.3*
$V_{h\,activation}$ (mV)	−13.1±0.5	−19.8±2.2*	−11.0±1.6	−15.3±2.3**	−9.0±1.6	−14.1±0.1**
$k_{activation}$ (mV)	4.6±0.8	5.4±1.0*	5.0±0.3	4.9±0.3	4.7±0.2	4.9±0.4
Kv4.3	*Control*	*SP (1 μM)*	*Control*	*CA (1 nM)*	*Control*	*CA (100 nM)*
$\tau_{f\,inactivation}$ (ms)	21.1±3.8	15.4±2.8*	18.6±4.3	11.6±2.6*	18.9±1.7	9.1±1.2**
$V_{h\,inactivation}$ (mV)	−33.5±1.1	−35.5±1.2	−37.0±1.8	−40.8±1.6*	−31.8±1.7	−42.0±2.1**
$k_{inactivation}$ (mV)	5.4±0.1	5.7±0.2	5.4±0.4	5.5±0.3	5.4±0.4	5.3±0.2
Kv7.1 + minK	*Control*	*SP (10 μM)*	*Control*	*CA (1 nM)*	*Control*	*CA (100 nM)*
$V_{h\,activation}$ (mV)	17.1±4.3	18.7±4.8	16.9±4.2	15.9±4.0	29.4±2.4	28.2±7.1
$k_{activation}$ (mV)	12.1±3.0	14.8±1.9	14.8±0.8	14.5±1.1	13.4±1.6	12.2±1.1
$\tau_{f\,deactivation}$ (ms)	189±54	212±52	155±30	135±39	252±24	313±80
$\tau_{s\,deactivation}$ (ms)	812±154	1126±230*	1039±297	963±161	776±174	1941±490*

Data are mean±s.e.m. of 6–8 experiments. *$P<0.05$ and **$P<0.01$ vs control, respectively.

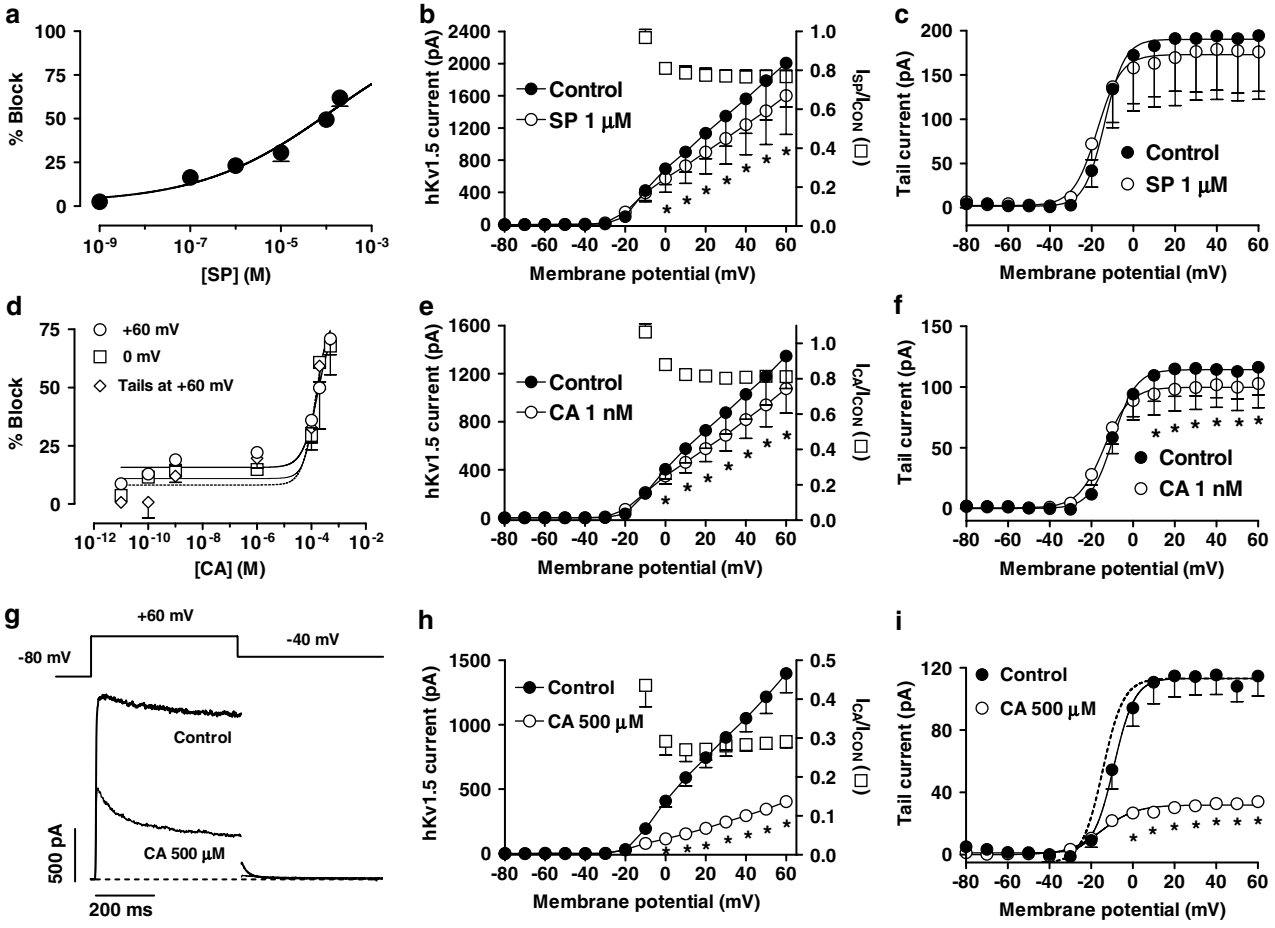

Figure 3 (a, d) Concentration–response relation for block of hKv1.5 channels in the presence of SP (a) and CA (d). The experimental data were fitted using the Hill equation. Each point represents the mean±s.e.m. of >5 experiments. (b, e, h) Averaged current–voltage relationship 500-ms isochronal, in the absence and presence of 1 μM SP (b), 1 nM CA (e) and 500 μM CA (h). Squares in these panels represent the fractional current block as a function of the membrane potential. (c, f, i) Averaged activation curves as calculated from the peak tail current amplitudes in the absence and presence of 1 μM SP (c), 1 nM CA (f) and 500 μM CA (i). In these panels, the continuous lines represent the fit of the data to a Boltzmann equation. In panels b, c, e, f, h, i, points represent the mean±s.e.m. of 6 experiments. In panel i, the dashed line represents the activation curve in the presence of 500 μM CA, normalised to the control amplitude. *$P<0.05$ vs control. (g) hKv1.5 current traces elicited by applying 500-ms pulses from −80 to +60 mV and tail currents recorded upon repolarisation to −40 mV in the absence and presence of 500 μM CA. The dashed line represents the zero current level.

Table 2 IC_{50}, n_H and B_{max} values obtained in the presence of CA on hKv1.5, Kv4.3 and Kv7.1 + minK channels

Current	*Index of block*	*IC_{50}*	n_H	B_{max} *(%)*
hKv1.5	+60 mV	173.5±21.6 μM	1.5±0.4	80.4±4.1
	0 mV	147.9±17.1 μM	2.0±0.7	77.1±4.3
	Tail at +60 mV	135.8±17.7 μM	1.8±0.8	78.7±5.7
Kv4.3	+50 mV	17.2±7.4 nM	0.6±0.2	79.9±21
	0 mV	2.6±1.3 nM	1.6±1.1	53.5±4.4
	Pulses to −30 mV	40.6±16.1 nM	0.4±0.06	93.3±4.7
Kv7.1 + minK	+40 mV	22.3±7.9 nM	0.3±0.4	78.9±28.8
	0 mV	29.6±18.0 nM	3.0±3.3	45.8±2.3
	Tail at +40 mV	0.7±0.4 μM	0.5±0.6	82.2±31.7

In hKv1.5 channels, the indexes of block used were the inhibition at the end of pulses to +60 and 0 mV, and of the tails recorded upon repolarisation to −40 mV after pulses to +60 mV (tail at +60 mV). In Kv4.3 channels, the indexes used were the reduction in the charge crossing the membrane after pulses to +50 and 0 mV, and in the peak current at +40 mV elicited after pulses to −30 mV (pulses to −30 mV). In Kv7.1 + minK channels, the indexes of block used were the inhibition of the current at the end of pulses to +40 and 0 mV, and of the tail currents recorded upon repolarisation to −40 mV after pulses to +40 mV (tail at +40 mV). Data are mean±s.e.m. of >5 experiments.

using the blockade at +60 mV as an index of block and the IC_{50} and n_H values appearing in Table 2.

Current–voltage relationships obtained in the absence and the presence of 1 μM SP and 1 nM CA are shown in Figures 3b and e, respectively. SP and CA significantly decreased the current amplitude at potentials positive to −10 mV ($P<0.05$). Squares in both panels represent the fractional current block as a function of the membrane potential. The results indicated that blockade appeared at the range of membrane potentials coinciding with that at which channel activation occurred and thereafter remained constant, reaching at +60 mV values of 23.2±3.2% ($n=5$) and 18.9±2.7% ($n=11$), in the presence of SP and CA, respectively. Figures 3c and f show the activation curves in the absence and presence of both drugs that were obtained by fitting by a Boltzmann equation, the tail current amplitudes plotted as a function of the membrane potential. SP slightly and CA significantly decreased the tail current amplitude at potentials positive to 0 mV, and both drugs shifted the midpoint (V_h) of the curve to more hyperpolarised potentials (Table 1). SP, but not CA, significantly modified the slope factor of the activation curve (Table 1). To better appreciate the voltage- and time-dependent effects produced by CA, Figures 3g–i show hKv1.5 current traces, the current–voltage relationships and the activation curves in the absence and the presence of 500 μM CA. At this concentration, the drug markedly inhibited the current at potentials between 0 and +60 mV, reaching a value of 70.9±15.4% of block at the end of pulses to +60 mV ($n=5$), slowed the time course of tail current deactivation and shifted the midpoint of the activation curve to more negative potentials (Table 1).

Effects of SP and CA on Kv4.3 currents

Figures 4a and b show Kv4.3 current traces obtained after 250-ms pulses to +50 mV under control conditions and in the presence of 1 μM SP and 1 nM CA. Kv4.3 currents rose rapidly to a peak ($\tau_{act}=1.1\pm0.1$ ms at +50 mV, $n=12$) and then inactivated according to a biexponential process. SP and CA decreased the peak amplitude and accelerated the fast phase of the current decay (Table 1) without modifying the slow phase ($\tau_{slow}=71.9\pm7.8$ ms, $n=10$) of the process. Furthermore, neither SP (1.1±0.1 ms, $n=6$) nor CA (1.0±0.1 ms, $n=6$) modified the time course of Kv4.3 channel activation. The blocking effects, but not the kinetics, were reversible in a 96.1±2.3 and 95.8±3.1%, respectively, upon washout of SP (Figure 4a) and CA (Figure 4b). Development of SP- and CA-induced block, analysed as was described above, was fitted to a monoexponential function and no block was observed before the channels opened, the τ_{Block} averaging 125±65 and 123±42 ms, respectively (Figures 4c and d).

The acceleration of the Kv4.3 current decline induced by SP and CA was suggestive of an open-channel block, and thus the reduction of peak current would not represent the steady-state block. Therefore, the reduction of the total charge crossing the membrane was estimated from the integral of the current traces elicited at +50 mV and fitted to the Hill equation (Figures 4e and f). Using this index of block, the fit yielded IC_{50} and n_H values of 47.1±15.8 and 0.4±0.09 μM, and 17.2±7.4 and 0.6±0.2 nM for SP and CA, respectively. Surprisingly, at CA concentrations ⩾1 μM the blockade did not increase but decreased, and thus these data points were not fitted. Similar results were obtained when the reduction in the charge crossing the membrane at 0 mV was used as an index of block. The reduction of the current amplitude obtained after conditioning pulses to −30 mV was also plotted as a function of the CA concentration (Figure 4f). As can be observed, between 0.01 and 500 nM, the blockade increased as the concentration of the drug was augmented, whereas at higher concentrations the blockade decreased. The IC_{50} and the n_H values obtained are given in Table 2.

Figure 5a shows representative Kv4.3 current traces obtained with the protocol used to assess the voltage dependence of activation and inactivation. The protocol consists of 250-ms conditioning pulses to potentials ranging between −90 and +50 mV, followed by a test pulse to +40 mV. In Figures 5b and c, the peak current–voltage relationship, constructed by plotting the peak current amplitude elicited by the conditioning pulse as a function of the membrane potential, demonstrated that 1 μM SP and 1 nM CA significantly decreased the Kv4.3 current at positive potentials. Squares in both panels represent the fractional current block. The SP-induced block decreased from 25.5±4.6% at 0 mV to 17.7±1.4% at +50 mV ($n=10$, $P<0.05$), whereas the CA-induced block remained constant in this range of potentials (15.6±3.3% at +50 mV, $n=10$, $P<0.05$). The total Kv4.3 charge as a function of the potential of the test pulse in the

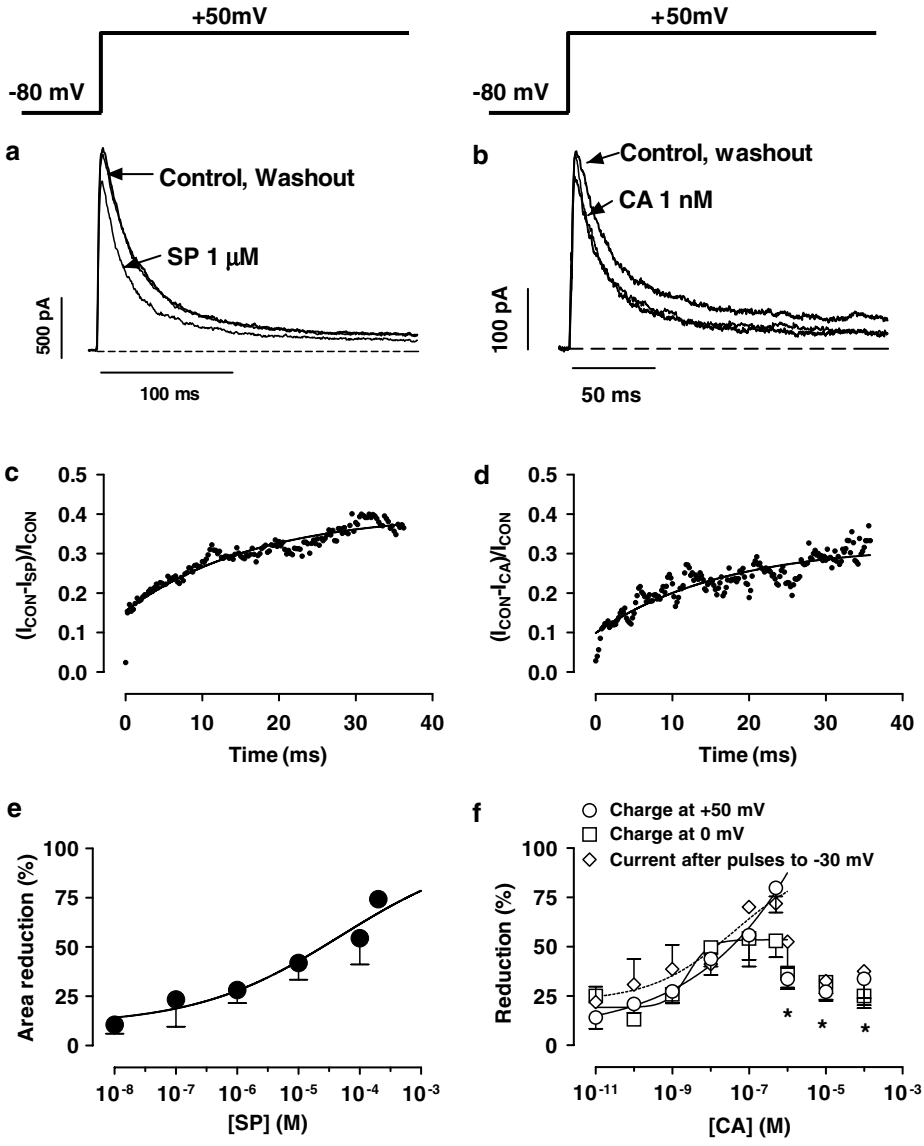

Figure 4 (a, b) Kv4.3 current traces obtained by applying 250-ms pulses to +50 mV in the absence, presence and after the washout of 1 μM SP (a) and 1 nM CA (b). (c, d) Plot of the current ratio between the SP- and CA-sensitive currents during the pulse to +50 mV ($I_{CON}-I_{SP}$ and $I_{CON}-I_{CA}$, respectively) and the current in control conditions. The continuous line represents the fit to a monoexponential function to obtain the τ_{block}. (e, f) Concentration-dependent effects of SP (e) and CA (f). In panel f, blockade has been measured as the reduction in the charge crossing the membrane after pulses to +50 and 0 mV or in the peak current amplitude obtained with pulses to +40 mV after prepulses to −30 mV. Data obtained between 0.01 and 500 nM were fitted using the Hill equation. *$P<0.05$ vs blockade obtained with 500 nM CA. In panels e, f, each point represents the mean ± s.e.m. of >5 experiments.

absence and the presence of SP and CA was plotted in Figures 5d and e, respectively. The total charge crossing the membrane was estimated from the integral of the current traces elicited at each membrane potential. Both drugs significantly decreased the charge crossing the membrane at potentials positive to −10 mV ($n=10$, $P<0.05$). The fractional charge block produced by SP (squares) decreased at potentials between −20 and +50 mV from 40.5±9.4 to 27.1±6.4% ($n=10$, $P<0.05$), whereas it remained constant in the presence of CA (27.4±5.7% at +50 mV, $n=10$, $P<0.05$). To construct the availability curves, the peak current amplitude elicited by the test pulse was plotted against the membrane potential of the conditioning pulse, and the data were fitted by a Boltzmann function. Figures 5f and g show the availability curves in the absence and the presence of SP and CA, respectively. SP decreased the peak Kv4.3 current amplitude, whereas it did not modify the V_h of the curve (Table 1). In contrast, CA shifted the V_h of the curve to more negative potentials (Table 1). Furthermore, CA-induced block reached statistical significance only at potentials positive to −50 mV, the potential at which most of the channels are in the inactivated state. These results suggested that CA, but not SP, also binds to the inactivated state of the Kv4.3 channels.

Effects of SP and CA on Kv7.1 + minK currents

Figure 6 shows families of current traces obtained by applying 2-s pulses from −80 mV to voltages between −80 and +40 mV

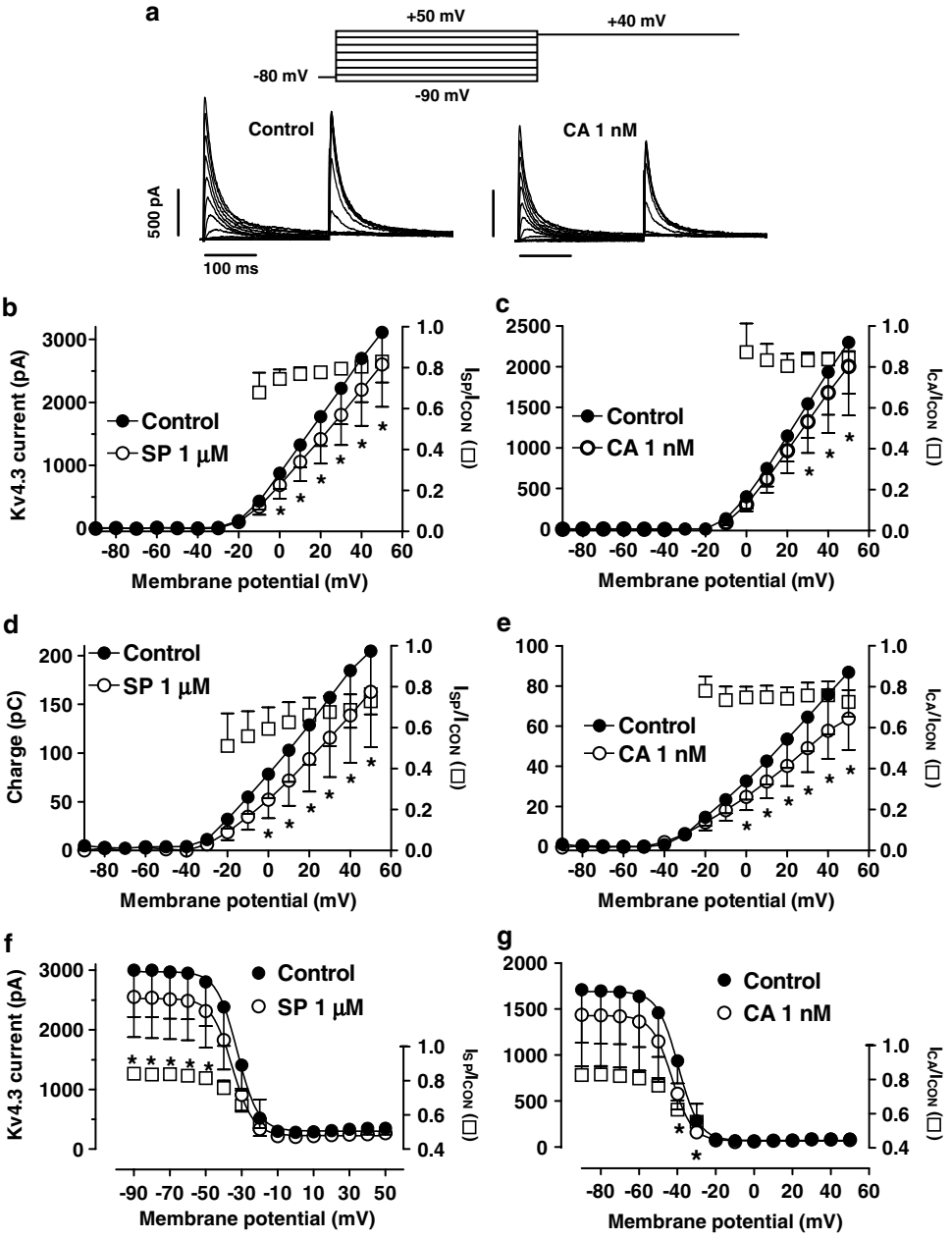

Figure 5 (a) Kv4.3 current traces in the absence and in the presence of 1 nM CA obtained when applying pulses to potentials ranging from −90 to + 50 mV followed by a 250-ms pulse to + 40 mV. (b, c) Peak current–voltage Kv4.3 relationship in the absence and presence of SP (b) and CA (c). (d, e) Relationship between the current–time integral and the membrane potential in the absence and presence of SP (d) and CA (e). (f, g) Inactivation curves in the absence and presence of SP (f) and CA (g) obtained by plotting the peak outward current elicited by the test pulse to + 40 mV as a function of the potential of the conditioning pulse. Continuous lines represent the fit of the data to a Boltzmann equation. In panels b–f, $*P<0.05$ vs control data. In panel g, $*P<0.05$ vs data obtained at −90 mV. In panels b–g, squares represent the fractional block as a function of the membrane potential and each point represents the mean ± s.e.m. of 10 experiments.

in 10 mV increments for control conditions and after perfusion of 10 μM SP (panel b) and 1 nM CA (panel c). Tail currents were recorded on repolarisation to −40 mV for 2 s. SP and CA decreased the outward and the tail Kv7.1 + minK currents, and these effects were almost completely reversed after washout (in 98.4 ± 2.6 and 98.7 ± 2.7%, respectively) (Figure 6a). Kv7.1 + minK current activation is a sigmoidal process, but, in order to describe the dominant time constants of the activation, an exponential analysis was used, fitting the traces to + 40 mV by a monoexponential function. SP, but not CA, slowed the time course of current activation, increasing the time constant of the process ($\tau_{actC} = 1.0 \pm 0.2$ s, $\tau_{actSP} = 1.8 \pm 0.6$ s, $n = 6$, $P<0.05$). The tail current decline was fitted to a biexponential (Table 1). Again SP, but not CA, slowed the time course of tail current deactivation, increasing the time constant of the slow phase of the process (Table 1). The current ratios between SP- and CA-sensitive currents during depolarising pulses to + 40 mV and the current in

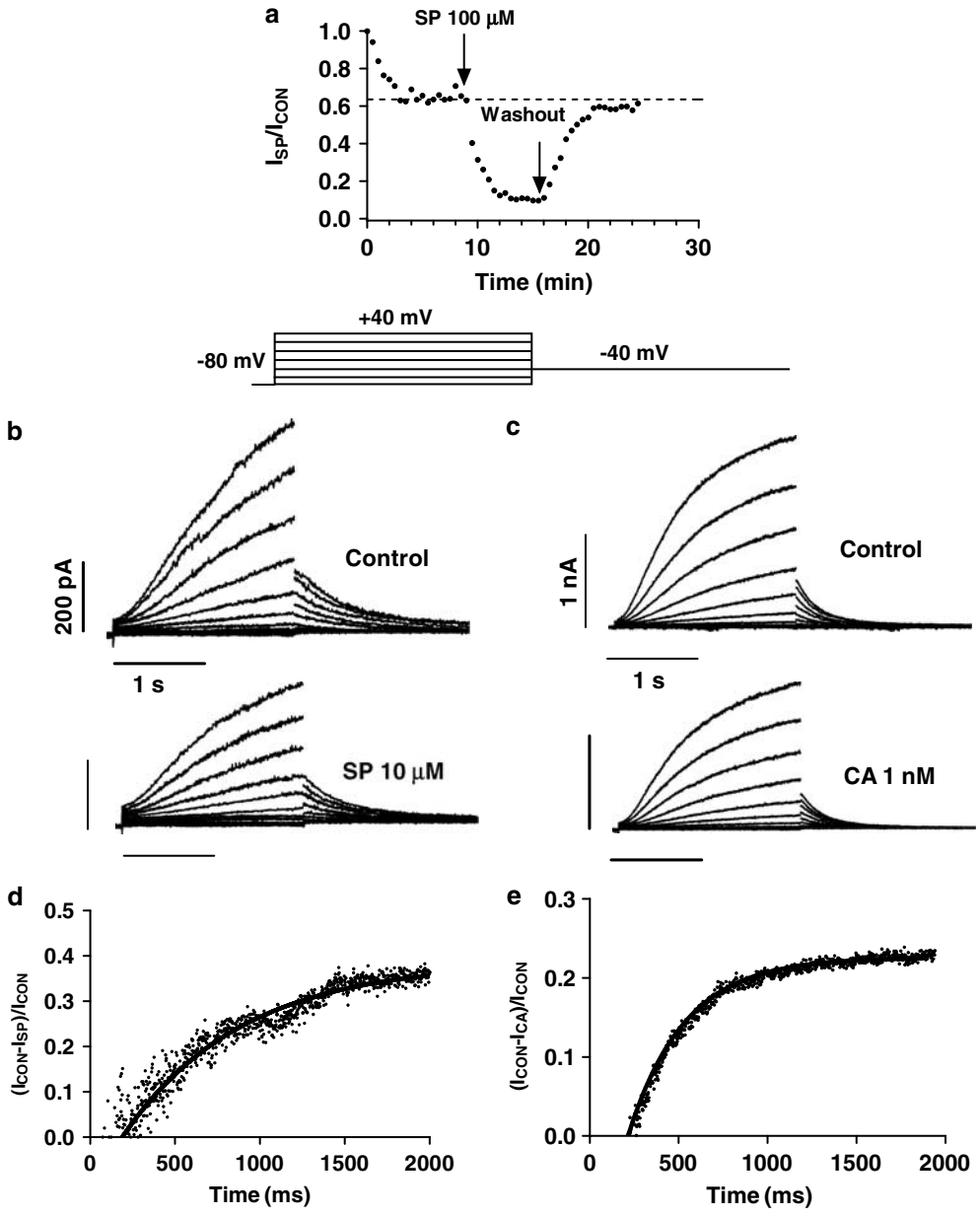

Figure 6 (a) Plot of the Kv7.1 + minK current amplitude elicited by 2-s pulses to +40 mV just after seal breaking and when the current amplitude reached steady state (control conditions, dotted line), as well as in the presence and following the washout of 100 μM SP. The arrows indicate the beginning and end of the superfusion with drug-containing solution, respectively. (b, c) Kv7.1 + minK current traces obtained with the voltage protocol illustrated in the upper part for control conditions and with 10 μM SP (b) or 1 nM CA (c). (d, e) Plot of the current ratio between the SP- and CA-sensitive currents during the pulse to +40 mV ($I_{CON}-I_{SP}$ and $I_{CON}-I_{CA}$, respectively) and the current in control conditions. The continuous line represents the fit to a monoexponential function to obtain the τ_{block}.

control conditions are shown in Figures 6d and e, respectively. In both cases, no block was observed before the depolarisation and the blockade increased during the application of the pulse. The τ_{Block} in the presence of 10 μM SP and 1 nM CA averaged 350±68 and 250±46 ms, respectively.

The reduction of the current at +40 mV was fitted to the Hill equation, and yielded IC_{50} and n_H values of 24.1±6.7 and 0.6±0.1 μM, and 22.3±7.9 and 0.3±0.4 nM for SP and CA, respectively (Figures 7a and d). Blockade produced by CA was also measured at the end of pulses to 0 mV and at the peak tail currents elicited after pulses to +40 mV. The IC_{50} and the n_H values obtained are given in Table 2.

Current–voltage plots of steady-state current present at the end of the 2-s depolarising steps (current–voltage relationship) and peak tail current (activation curve) are depicted in panels b, c, e and f of Figure 7. In the presence of 10 μM SP, steady-state current amplitude elicited at +40 mV was reduced by 38.6±2.3% ($n=6$, $P<0.05$). SP significantly decreased the tail current amplitude elicited at positive potentials, but did not modify the voltage dependence of Kv7.1 + minK channel activation (panel c, continuous lines, Table 1). Squares in panels b and c represent the fractional block as a function of membrane potential. The results indicated that blockade appeared at the range of membrane potentials coinciding with

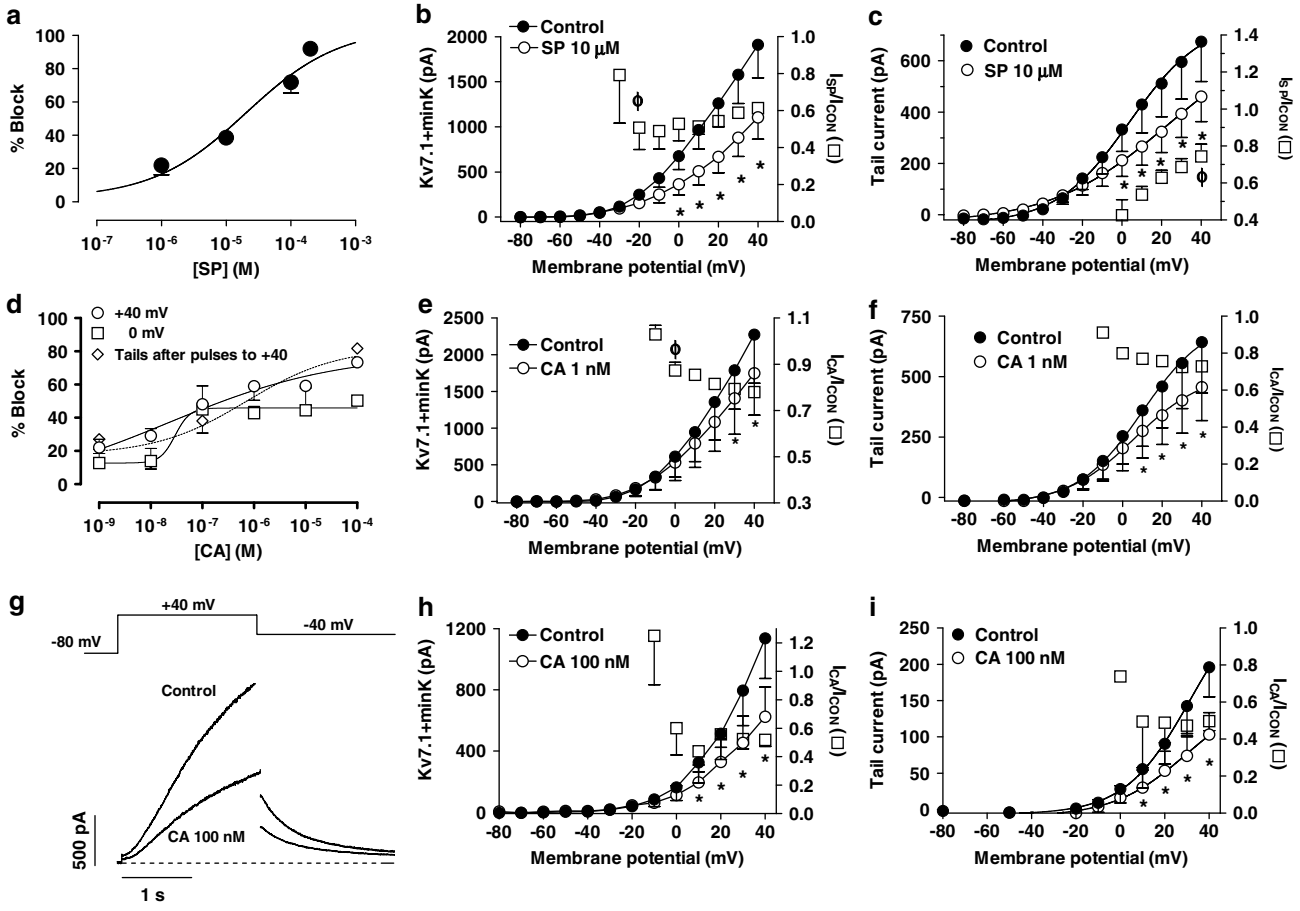

Figure 7 (a, d) Concentration-dependent effects of SP (a) and CA (d) on Kv7.1 + minK currents. Data were fitted using the Hill equation. Each point represents the mean ± s.e.m. of >5 experiments. (b, e, h) Averaged current–voltage Kv7.1 + minK relationships 2-s isochronal in the absence and presence of 10 μM SP (b), 1 nM CA (e) and 100 nM CA (h). (c, f, i) Averaged activation curves as calculated from the peak tail current amplitudes under control conditions and in the presence of 10 μM SP (c), 1 nM CA (f) and 100 nM CA (i). In these panels, the continuous lines represent the fit of the data to a Boltzmann equation. In panels b, c, e, f, h, i, squares represent the fractional block as a function of the membrane potential and symbols the mean ± s.e.m. of 6 experiments. *$P<0.05$ vs control; ϕ, $P<0.05$ vs data at +40 mV (b, e) or at 0 mV (c). (g) Kv7.1 + minK current traces elicited by applying 2-s pulses from −80 to +40 mV and tail currents recorded upon repolarisation to −40 mV in the absence and presence of 100 nM CA. The dashed line represents the zero current level.

that at which channel activation occurred, and, thereafter, it decreased progressively. In fact, tail current block decreased from 52.0 ± 9.2% at 0 mV to 25.6 ± 3.3% at +40 mV ($n=6$, $P<0.05$).

CA (1 nM) decreased the outward current at the end of the 2-s pulse to +40 mV (Figure 7e) by 22.1 ± 1.4% and the tail current elicited on return to −40 mV (Figure 7f) by 27.1 ± 1.9%, but did not modify the voltage dependence of Kv7.1 + minK channel activation (panel f, continuous lines, Table 1). Squares in panels e and f represent the fractional block as a function of membrane potential. The results indicated that blockade appeared at the range of membrane potentials, coinciding with that at which channel activation occurred, and, thereafter, it increased progressively. When CA concentration was raised to 100 nM, the drug reduced the current at the end of pulses to +40 mV by 48.1 ± 11.0% ($n=5$) (Figure 7g), and the peak tail current amplitude by 50.3 ± 5.1%. At this concentration, CA slowed the time course of current deactivation (Table 1) without modifying the voltage dependence of Kv7.1 + minK channel activation (Figure 7i). As was observed with 1 nM, the blockade appeared at the range of potentials of channel opening, suggesting an open-channel interaction (Figures 7h and i).

Effects of CA on native K+ currents

Figure 8a shows representative outward K^+ currents recorded in mouse ventricular myocytes by applying 250-ms pulses from −80 to +50 mV under control conditions, in the presence of 50 μM 4-aminopyridine alone, and plus 1 nM CA. At this concentration, 4-aminopyridine selectively inhibited I_{Kur} (Wang *et al*., 1993; Brouillette *et al*., 2004; Brunet *et al*., 2004; Tamargo *et al*., 2004), leaving a transient current that rapidly activated and decayed to a constant level at the end of the pulse. Superfusion of 4-aminopyridine plus CA inhibited the current (measured as the difference between peak outward and end-pulse current) by 16.1 ± 3.9%, without affecting the time course of current decay ($\tau_f = 19.4 \pm 2.2$ ms and $\tau_s = 199.2 \pm 32.1$ ms, $n=5$, $P>0.05$). We next studied the effects of CA on I_{Kur}, also recorded in mouse ventricular myocytes. A 200-ms prepulse to +40 mV to inactivate I_{to1} was applied, followed by a 500-ms pulse to +50 mV, eliciting a

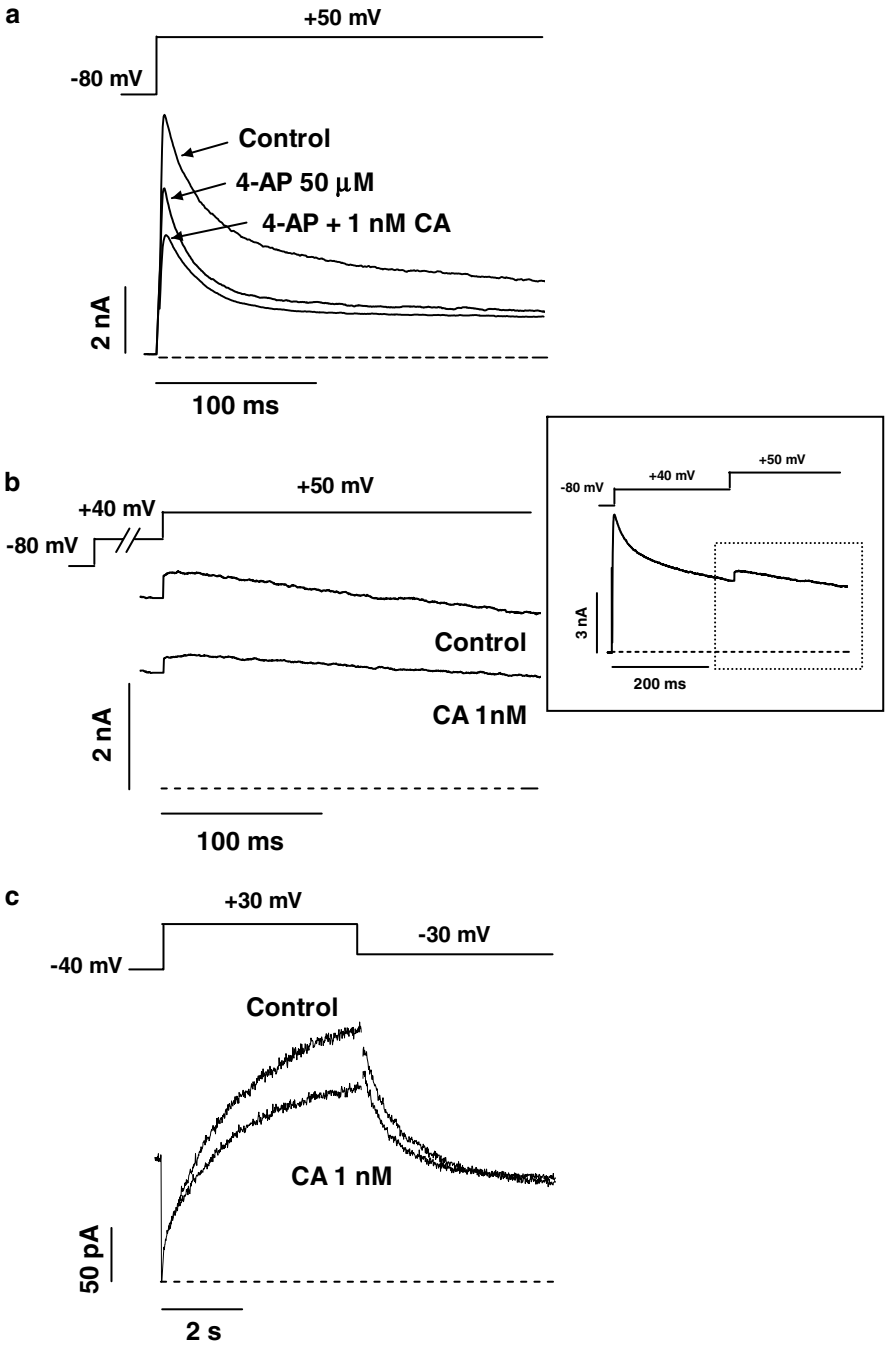

Figure 8 (a) Outward K^+ currents recorded in a mouse ventricular myocyte elicited by applying 250-ms pulses from −80 to +50 mV under control conditions, and in the presence of 50 μM 4-aminopyridine alone and plus 1 nM CA. (b) Outward K^+ currents recorded in a mouse ventricular myocyte elicited by applying 500-ms pulses to +50 mV in the absence and presence of 1 nM CA. A 200-ms prepulse to +40 mV was applied in order to isolate the I_{Kur} (see inset). (c) Maximum outward I_K recorded in guinea-pig ventricular myocytes elicited by applying 5-s pulses from −40 to +30 mV and tail currents obtained upon repolarisation to −30 mV in the absence and presence of 1 nM CA.

slowly inactivating delayed rectifier outward K^+ current, which is composed of the sum of at least two components, where only the I_{Kur} component carried by Kv1.5 channels exhibits slow inactivation (Brunet *et al*., 2004). CA inhibited the current (measured as the difference between the peak current and the current at the end of the pulse) elicited by the pulse to +50 mV by 29.2±5.5% (Figure 8b). In another group of experiments, the effects of CA on I_K recorded in isolated guinea-pig ventricular myocytes were analysed. Figure 8c shows I_K traces recorded by applying 5-s pulses to +30 mV and tail currents elicited upon repolarisation to −30 mV in the absence and the presence of 1 nM CA. In guinea-pig myocytes, I_K is composed of a rapidly activating component (I_{Kr}) and a slowly activating component (I_{Ks}) (Delpón *et al*., 1995). I_{Kr} activates rapidly with moderate depolarisations (between −40 and 0 mV), whereas I_{Ks} activates slowly with a sigmoidal time

course at more positive potentials. Thus, at the end of the pulse to +30 mV, mainly I_{Ks} would be present and CA inhibited this current by 21.8±6.9% ($n=5$). Upon repolarisation to −30 mV, the tail current obtained is mainly due to I_{Kr}, because of the inward rectifying properties of this current. For this reason, CA-induced block measured at the peak of the tail currents only reached a 12.1±3.9%.

Mathematical modelling of a human atrial action potential

We ran a previously described model of a human atrial action potential (Courtemanche *et al*., 1999) by incorporating the experimentally measured blockade values and effects on the kinetics induced by CA 1 nM on Kv4.3, hKv1.5 and Kv7.1 + minK, as well as those obtained on Kv11.1 (HERG) channels (Caballero *et al*., 2003). Figures 9a and b show the theoretical effects of CA 1 nM on the normal and AF-modified action potentials, respectively. In normal conditions, CA slowed phase 1 of repolarisation and markedly increased the plateau to more positive potentials as a consequence of the blockade of Kv4.3 and hKv1.5 channels. Inhibition of HERG and Kv7.1 + minK currents led to a lengthening of the APD measured at 50% (APD_{50}) and 90% (APD_{90}) of repolarisation of 22.6 and 8.2%, respectively (Figure 9c). In AF simulated conditions, the APD was shorter compared to normal conditions as a consequence of the electrical remodelling. Under these conditions, CA-blocking effects on the respective currents resulted in a lengthening of the APD_{90} of 10.2% (Figure 9d).

Discussion

Our results demonstrate for the first time that SP and its metabolite CA directly block cardiac hKv1.5, Kv4.3 and Kv7.1 + minK channels. Moreover, CA inhibited native I_{to1}, I_{Kslow1} and I_K currents to extents similar to Kv4.3, hKv1.5 and Kv7.1 + minK currents. It should be stressed that the experiments were carried out in the absence of aldosterone, and thus the blockade is not attributable to antagonism of the aldosterone effects at the receptor level. Furthermore, both CA and aldosterone blocked the native I_{Ks} and I_{Kr} currents (Caballero *et al*., 2003). These latter results add further support to the hypothesis of a direct interaction of SP and CA with the channel protein, since the blocking effects of aldosterone should be reversed by the aldosterone receptor antagonists SP and CA. However, a further blockade was induced. The concentration-dependent effects of SP and, particularly, of CA on Kv4.3, hKv1.5 and Kv7.1 + minK channels were unusual and the n_H values obtained suggested that a complex interaction between the CA molecule(s) and the channel proteins was produced. Furthermore, even when a wide range of CA concentrations was tested, none of the concentration–response curves reached saturation. However, this fact cannot be resolved by further increasing the drug concentration because this implies exposing the cells to a high methanol concentration. It should be stressed that in all three channels, even when different parameters were used as an index of CA block, the shape of the concentration–response curves was conserved. The unusual concentration–response curves were not attributable to an unspecific time-dependent

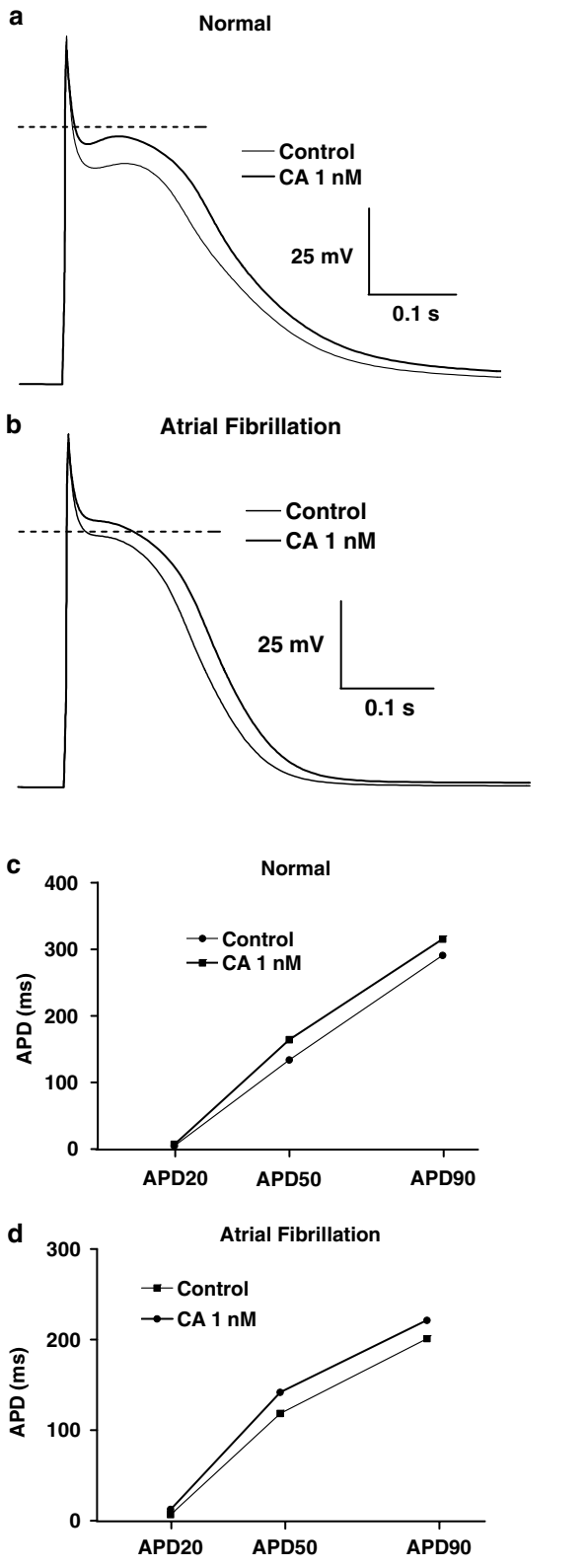

Figure 9 (a, b) Model APs under normal (a) and AF simulated (b) conditions in the absence and presence of 1 nM CA. (c, d) Action potential duration under normal (c) and AF simulated (d) conditions measured at 20, 50 and 90% of repolarisation in the absence and presence of 1 nM CA.

decrease of current amplitudes, since under our experimental conditions hKv1.5, Kv4.3 and Kv7.1 + minK currents remained unchanged during the time of recordings (25–30 min) (Caballero *et al*., 2004). Furthermore, the washout of the blocking effects was carefully tested in all the experiments. In this context, it could be asserted that the resultant order of potency of block of CA in the studied channels was Kv4.3 > Kv7.1 + minK ≫ hKv1.5. However, it should be considered that the maximum level of block produced by CA was different in all three channels, that is, the efficacy of block was different. The concentration-dependent effects of CA on Kv11.1 channels were also unusual ($IC_{50} = 105\,\mu$M), since the blockade remained constant over a wide range of concentrations (from 0.01 nM to 0.1 μM) (Caballero *et al*., 2003). To describe the drug–channel interaction, we used the most common model in which the drug molecule interacts with the receptor in a reversible bimolecular reaction with the formation of a drug–receptor complex. This model obeys simple mass action principles (a reversible, saturable and one-to-one interaction between ligand and receptor) (Christopoulos & Kenakin, 2002). However, this simplest model is not often compatible with experimental observations, since the Hill equation is not a physically realistic reaction scheme (Weiss, 1997). The singular CA concentration-dependent effects could reflect the existence of at least two topographically distinct binding sites on the channel proteins that are negatively/positively coupled (allosteric interactions). Thus, binding of one CA molecule to a receptor site would decrease/increase the affinity for the binding to the other nonoccupied site (Waud, 1968). This might particularly account for the decrease in block observed in Kv4.3 channels at concentrations $\geqslant 1\,\mu$M. However, we cannot rule out other explanations, such as CA promoting the isomerisation of the receptor protein between multiple conformational states with different affinities (allosteric transition) (Christopoulos & Kenakin, 2002) or the existence of steric hindrance interactions between bulky CA molecules near the binding site.

In the presence of SP, the n_H values obtained were below unity. However, in all the three channels the blockade increased monotonically when the SP concentration was increased. The resultant order of potency of block of SP was different from that of CA: Kv7.1 + minK > Kv4.3 > hKv1.5.

State dependence of the CA and SP effects

The CA-induced block of hKv1.5 and Kv7.1 + minK increased in the voltage range of channel activation, suggesting that CA blocks the open state of these channels. Thereafter, at potentials at which channel activation reached saturation, CA-induced block significantly increased in Kv7.1 + minK, whereas it remained constant in hKv1.5 channels. CA slowed the time course of tail current decline in hKv1.5 channels, thus inducing a 'crossover phenomenon', whereas it did not modify the kinetics of this process in Kv7.1 + minK channels. This latter result, however, did not exclude the open-state interaction but suggested that the dissociation of CA during the hyperpolarisation (not studied) was faster than the channel closing. In Kv4.3 channels, CA shifted the availability curve, the blockade increasing with the channel inactivation, which indicated that CA blocked the inactivated state of the channel. At the same time, CA accelerated the Kv4.3 current decline, which is suggestive of an open-channel block mechanism (Caballero *et al*., 2004). Furthermore, the analysis of the development of CA-induced block demonstrated that, in all three channels, the blockade developed after channel opening and that no block was observed at the early beginning of the depolarising pulse. These results add further support to the proposed open-state interaction. However, the monoexponential increase of hKv1.5 channels block during the depolarisation did not exclude the interaction of CA with the slow inactivated state of the hKv1.5 channel. In fact, a monoexponential increase was also observed in Kv4.3 channels in which CA blocked both the open and the inactivated states of the channels. Development of CA-induced block in Kv7.1 + minK channels was faster than SP-induced block and even faster than the activation kinetics of the channel. Thus, it would be expected that Kv7.1 + minK currents were simply scaled down by CA, without any noticeable effect on their activation kinetics. These results, which were similar to those previously reported with propafenone on native I_{Ks} (Delpón *et al*., 1995), suggested that CA probably binds to conformational states that appear during transitions between the rested and open states of the channel.

SP-induced block of hKv1.5 and Kv7.1 + minK also increased in the voltage range of channel activation and thereafter decreased at potentials at which channel activation reached saturation. In all the three channels, the blockade developed after channels started opening and no block before opening was observed. Furthermore, SP slowed the tail current declines of hKv1.5 and Kv7.1 + minK channels, and accelerated the Kv4.3 current decline. All these observations indicated that SP preferentially blocks the open state of these three cardiac K^+ channels. However, the importance of these results was precluded by that fact that SP is metabolised too rapidly to be detected in plasma (Karim, 1978).

Clinical implications

SP is rapidly metabolised (half-life ≈ 1.5 h), whereas its metabolites (canrenone and/or CA) have considerably longer half-life values (≈ 16.5 h). The peak plasma concentration of canrenone after administration of therapeutic doses of SP ranges between 0.3 and 1.6 μM (Karim, 1978). Canrenone is extensively bound (98%) to plasma proteins and is in enzymatic equilibrium with CA, producing peak free plasma concentrations of CA of 3–16 nM (Karim, 1978). Therefore, the present study demonstrates that at therapeutic concentrations CA blocks hKv1.5, Kv4.3 and Kv7.1 + minK in addition to Kv11.1 (Caballero *et al*., 2003) and L-type Ca^{2+} channels (Dacquet *et al*., 1987). Two old studies demonstrated that SP and CA lengthened the duration and refractoriness of the cardiac action potentials (Briggs & Holland, 1959; Coraboeuf & Deroubaix, 1974) recorded in rabbit and rat multicellular preparations, effects that were empirically attributed to a decrease in K^+ conductance (Coraboeuf & Deroubaix, 1974). The blockade of the cloned cardiac potassium channels was reproduced in native I_{to1}, I_{Kur} and I_{Ks}, as was previously demonstrated for CA on Kv11.1 and I_{Kr} currents (Caballero *et al*., 2003), and might account for the described lengthening. In fact, using the mathematical modelling, we have shown that CA would prolong human atrial action potential duration both in normal and in AF-modified conditions. *In vivo* the CA effects on Kv11.1 channels and cardiac repolarisation might be blunted, since SP produces hyperkalaemia (Kim, 1996) and,

unlike most other K^+ currents, Kv11.1 current amplitude increases upon elevation of $[K^+]_o$ (Yang & Roden, 1996). In fact, SP decreased QTc and QT dispersion in patients with congestive heart failure (Yee *et al*., 2001). However, it is not expected that hyperkalaemia would reduce the blocking effects of CA on hKv1.5, Kv4.3 and Kv7.1 + minK currents; instead, a further decrease would be produced. On the other hand, it has been very recently demonstrated that acute intravenous administration of aldosterone in patients with supraventricular arrhythmias after radiofrequency ablation increased the duration of the monophasic action potentials recorded in the right atrium (Tillmann *et al*., 2002). The fast onset of the prolonging effects led to the proposal that the effect of aldosterone cannot be mediated genomically. Thus, if the lengthening effects of aldosterone are not mediated by its interaction with the aldosterone receptors, it is not expected that the administration of the aldosterone receptor antagonists SP and CA can counteract its prolonging effects.

AF is associated with the activation of the renin–angiotensin system (Li *et al*., 2001), and angiotensin-converting enzyme inhibitors and angiotensin II type 1 receptor antagonists reduced the risk of developing and the recurrences of AF associated with hypertension and congestive heart failure (Madrid *et al*., 2004; Zaman *et al*., 2004). However, neither angiotensin-converting enzyme inhibition nor angiotensin receptor blockade fully suppress aldosterone production, a phenomenon designated as aldosterone escape (Struthers, 1995). Aldosterone levels are elevated in patients with persistent AF, which may produce proarrhythmic effects by several mechanisms and is involved in cardiac remodelling (Goette *et al*., 2001; Stier *et al*., 2002). In fact, aldosterone produces cellular electrophysiological alterations, including the decrease in the expression of voltage-dependent K^+ channels (Stier *et al*., 2002), particularly those that generated the I_{to1} (Benitah *et al*., 2001). Under these conditions, it can be speculated that aldosterone antagonists such as SP may ameliorate atrial remodelling and add further benefit to reduce AF recurrences (Korantzopoulos *et al*., 2004).

The present results demonstrated that CA, at therapeutic concentrations, directly blocks cardiac hKv1.5, Kv4.3 and Kv7.1 + minK channels, and, as a consequence, a prolongation of the human atrial APs and refractoriness would be produced. Blockade of cardiac K^+ currents exclusively (I_{Kur}) or predominantly (I_{to1}) (Bertaso *et al*., 2002) present in the atria, together with the antagonism of the aldosterone proarrhythmic effects produced by SP (Brilla *et al*., 1993; Stier *et al*., 2002), might be highly desirable for the treatment of supraventricular arrhythmias. In fact, we demonstrated that irbesartan at therapeutic free plasma concentrations blocked hKv1.5 and Kv4.3 channels (Moreno *et al*., 2003), an effect that might contribute to the decrease in the recurrence of AF in patients treated with amiodarone after cardioversion (Madrid *et al*., 2002). Further studies, however, are needed to fully analyse the resultant effects of SP/CA on human atrial repolarisation and their possible clinical implications.

We thank Drs MM Tamkun, DJ Snyders, M Keating and M Sanguinetti for providing hKv1.5, Kv4.3 and Kv7.1 + minK clones. We also thank Guadalupe Pablo for her excellent technical assistance. This work was supported by CICYT (SAF2002-02304), CAM (GR/SAL/0897/2004), Red RECAVA and Pfizer Foundation Grants.

References

ANTZELEVITCH, C. & FISH, J. (2001). Electrical heterogeneity within the ventricular wall. *Basic Res. Cardiol.,* **96,** 517–527.

BENITAH, J.P., PERRIER, E., GÓMEZ, A.M. & VASSORT, G. (2001). Effects of aldosterone on transient outward K^+ current density in rat ventricular myocytes. *J. Physiol.,* **537,** 151–160.

BERTASO, F., SHARPE, C., HENDRY, B. & JAMES, A.F. (2002). Expression of voltage-gated K^+ channels in human atrium. *Basic Res. Cardiol.,* **97,** 424–433.

BRIGGS, A. & HOLLAND, W. (1959). Antifibrillatory effects of electrolyte regulating steroids on isolated rabbit atria. *Am. J. Physiol.,* **197,** 1161–1164.

BRILLA, C.G., MATSUBARA, L.S. & WEBER, K.T. (1993). Antifibrotic effects of spironolactone in preventing myocardial fibrosis in systemic arterial hypertension. *Am. J. Cardiol.,* **71,** 12–16.

BROUILLETTE, J., CLARK, R.B., GILES, W.R. & FISET, C. (2004). Functional properties of K^+ currents in adult mouse ventricular myocytes. *J. Physiol.,* **559,** 777–798.

BRUNET, S., AIMOND, F., LI, H., GUO, W., ELDSTROM, J., FEDIDA, D., YAMADA, K.A. & NERBONNE, J.M. (2004). Heterogeneous expression of repolarising, voltage-gated K^+ currents in adult mouse ventricles. *J. Physiol.,* **559,** 103–120.

CABALLERO, R., DELPÓN, E., VALENZUELA, C., LONGOBARDO, M., GONZÁLEZ, T. & TAMARGO, J. (2001). Direct effects of candesartan and eprosartan on human cloned potassium channels involved in cardiac repolarization. *Mol. Pharmacol.,* **59,** 825–836.

CABALLERO, R., GÓMEZ, R., NÚÑEZ, L., MORENO, I., TAMARGO, J. & DELPÓN, E. (2004). Diltiazem inhibits hKv1.5 and Kv4.3 currents at therapeutic concentrations. *Cardiovasc. Res.,* **64,** 457–466.

CABALLERO, R., MORENO, I., GONZÁLEZ, T., ARIAS, C., VALENZUELA, C., DELPÓN, E. & TAMARGO, J. (2003). Spironolactone and its main metabolite, canrenoic acid, block human ether-a-go-go-related gene channels. *Circulation,* **107,** 889–895.

CARMELIET, E. (1992). Voltage- and time-dependent block of the delayed K^+ current in cardiac myocytes by dofetilide. *J. Pharmacol. Exp. Ther.,* **262,** 809–817.

CASTLE, N.A. (1990). Bupivacaine inhibits the transient outward K^+ current but not the inward rectifier in rat ventricular myocytes. *J. Pharmacol. Exp. Ther.,* **255,** 1038–1046.

CHRISTOPOULOS, A. & KENAKIN, T. (2002). G protein-coupled receptor allosterism and complexing. *Pharmacol. Rev.,* **54,** 323–374.

CORABOEUF, E. & DEROUBAIX, E. (1974). Effect of a spironolactone derivative, sodium canrenoate, on mechanical and electrical activities of isolated rat myocardium. *J. Pharmacol. Exp. Ther.,* **191,** 128–138.

COURTEMANCHE, M., RAMIREZ, R.J. & NATTEL, S. (1999). Ionic targets for drug therapy and atrial fibrillation-induced electrical remodeling: insights from a mathematical model. *Cardiovasc. Res.,* **42,** 477–489.

DACQUET, C., LOIRAND, G., MIRONNEAU, C., MIRONNEAU, J. & PACAUD, P. (1987). Spironolactone inhibition of contraction and calcium channels in rat portal vein. *Br. J. Pharmacol.,* **92,** 535–544.

DELPÓN, E., VALENZUELA, C., PÉREZ, O., CASIS, O. & TAMARGO, J. (1995). Propafenone preferentially blocks the rapidly activating component of delayed rectifier K^+ current in guinea pig ventricular myocytes. Voltage-independent and time-dependent block of the slowly activating component. *Circ. Res.,* **76,** 223–235.

DUAN, D., FERMINI, B. & NATTEL, S. (1993). Potassium channel blocking properties of propafenone in rabbit atrial myocytes. *J. Pharmacol. Exp. Ther.,* **264,** 1113–1123.

GOETTE, A., HOFFMANNS, P., ENAYATI, W., MELTENDORF, U., GELLER, J.C. & KLEIN, H.U. (2001). Effect of successful electrical cardioversion on serum aldosterone in patients with persistent atrial fibrillation. *Am. J. Cardiol.,* **88,** 906–909.

KARIM, A. (1978). Spironolactone: disposition, metabolism, pharmacodynamics, and bioavailability. *Drug Metab. Rev.,* **8,** 151–188.

KIM, K.E. (1996). Spironolactone. In: *Cardiovascular Drug Therapy,* ed. Messerli, F.H. pp. 454–460. Philadelphia: Saunders Co.

KORANTZOPOULOS, P., KOLETTIS, T., KOUNTOURIS, E. & SIOGAS, K. (2004). Atrial remodeling in persistent atrial fibrillation: the potential role of aldosterone. *Eur. Heart J.,* **25,** 1086.

LI, D., SHINAGAWA, K., PANG, L., LEUNG, T.K., CARDIN, S., WANG, Z. & NATTEL, S. (2001). Effects of angiotensin-converting enzyme inhibition on the development of the atrial fibrillation substrate in dogs with ventricular tachypacing-induced congestive heart failure. *Circulation,* **104,** 2608–2614.

LOUSSOUARN, G., PARK, K.H., BELLOCQ, C., BARO, I., CHARPENTIER, F. & ESCANDE, D. (2003). Phosphatidylinositol-4,5-bisphosphate, PIP2, controls KCNQ1/KCNE1 voltage-gated potassium channels: a functional homology between voltage-gated and inward rectifier K^+ channels. *EMBO J.,* **22,** 5412–5421.

MADRID, A.H., BUENO, M.G., REBOLLO, J.M., MARÍN, I., PENA, G., BERNAL, E., RODRÍGUEZ, A., CANO, L., CANO, J.M., CABEZA, P. & MORO, C. (2002). Use of irbesartan to maintain sinus rhythm in patients with long-lasting persistent atrial fibrillation: a prospective and randomized study. *Circulation,* **106,** 331–336.

MADRID, A.H., PENG, J., ZAMORA, J., MARÍN, I., BERNAL, E., ESCOBAR, C., MUNOS-TINOCO, C., REBOLLO, J.M. & MORO, C. (2004). The role of angiotensin receptor blockers and/or angiotensin converting enzyme inhibitors in the prevention of atrial fibrillation in patients with cardiovascular diseases. *Pacing Clin. Electrophysiol.,* **27,** 1405–1410.

MORENO, I., CABALLERO, R., GONZÁLEZ, T., ARIAS, C., VALENZUELA, C., IRIEPA, I., GÁLVEZ, E., TAMARGO, J. & DELPÓN, E. (2003). Effects of irbesartan on cloned potassium channels involved in human cardiac repolarization. *J. Pharmacol. Exp. Ther.,* **304,** 862–873.

NERBONNE, J.M. & GUO, W. (2002). Heterogeneous expression of voltage-gated potassium channels in the heart: roles in normal excitation and arrhythmias. *J. Cardiovasc. Electrophysiol.,* **13,** 406–409.

PITT, B., ZANNAD, F., REMME, W., CODY, R., CASTAIGNE, A., PEREZ, A., PALENSKY, J. & WITTES, J. (1999). The effect of spironolactone on morbidity and mortality in patients with severe heart failure. *N. Engl. J. Med.,* **341,** 709–717.

RAMIRES, F.J., MANSUR, A., COELHO, O., MARANHAO, M., GRUPPI, C.J., MADY, C. & RAMIRES, J.A. (2000). Effect of spironolactone on ventricular arrhythmias in congestive heart failure secondary to idiopathic dilated or to ischemic cardiomyopathy. *Am. J. Cardiol.,* **85,** 1207–1211.

SNYDERS, D., TAMKUN, M. & BENNETT, P. (1993). A rapidly activating and slowly inactivating potassium channel cloned from human heart. Functional analysis after stable mammalian cell culture expression. *J. Gen. Physiol.,* **101,** 513–543.

STIER, C.T., CHANDER, P.N. & ROCHA, R. (2002). Aldosterone as a mediator in cardiovascular injury. *Cardiol. Rev.,* **10,** 97–107.

STRUTHERS, A.D. (1995). Aldosterone escape during ACE inhibitor therapy in chronic heart failure. *Eur. Heart J.,* **16,** 103–106.

TAMARGO, J., CABALLERO, R., GÓMEZ, R., VALENZUELA, C. & DELPÓN, E. (2004). Pharmacology of cardiac potassium channels. *Cardiovasc. Res.,* **62,** 9–33.

TILLMANN, H.C., SCHUMACHER, B., YASENYEV, O., JUNKER, M., CHRIST, M., FEURING, M. & WEHLING, M. (2002). Acute effects of aldosterone on intracardiac monophasic action potentials. *Int. J. Cardiol.,* **84,** 33–39.

WANG, Z., FERMINI, B. & NATTEL, S. (1993). Sustained depolarization-induced outward current in human atrial myocytes. Evidence for a novel delayed rectifier K^+ current similar to Kv1.5 cloned channel currents. *Circ. Res.,* **73,** 1061–1076.

WAUD, D. (1968). Pharmacological receptors. *Pharmacol. Rev.,* **20,** 49–88.

WEISS, J.N. (1997). The Hill equation revisited: uses and misuses. *FASEB J.,* **11,** 835–841.

YANG, T. & RODEN, D. (1996). Extracellular potassium modulation of drug block of I_{Kr}. *Circulation,* **93,** 407–411.

YEE, K.M., PRINGLE, S. & STRUTHERS, A. (2001). Circadian variation in the effects of aldosterone blockade on heart rate variability and QT dispersion in congestive heart failure. *J. Am. Coll. Cardiol.,* **37,** 1800–1807.

ZAMAN, A.G., KEARNEY, M.T., SCHECTER, C., WORTHLEY, S.G. & NOLAN, J. (2004). Angiotensin-converting enzyme inhibitors as adjunctive therapy in patients with persistent atrial fibrillation. *Am. Heart J.,* **147,** 823–827.

(Received March 17, 2005
Accepted May 11, 2005
Published online 27 June 2005)